Journal of Wind Engineering & Industrial Aerodynamics 268 (2026) 106285

Contents lists available at ScienceDirect

Journal of Wind Engineering & Industrial Aerodynamics

journal homepage: www.elsevier.com/locate/jweia

A benchmark between two different numerical models for ice galloping prediction

Federico Zanelli [a,*], Giuseppe Bucca [a], Stefano Melzi [a], Sonia Zuin [a], Giorgio Diana [a], Saki Taruishi [b], Hisato Matsumiya [b,c]

[a] Department of Mechanical Engineering, Politecnico di Milano, Via La Masa 1, 20156, Milan, Italy
[b] Sustainable System Research Laboratory, Central Research Institute of Electric Power Industry, Abiko 1646, Abiko-shi, Chiba, 270-1194, Japan
[c] Department of Civil and Earth Resources Engineering, Kyoto University, Kyotodaigaku-katsura, Nishikyo-ku, Kyoto, 615-8540, Japan

ARTICLE INFO

Keywords:
Galloping
Ice shape
Bundle conductor
Quasi steady theory
Numerical simulation
Wind tunnel tests

ABSTRACT

Galloping is a wind-induced phenomenon which can lead conductors of transmission lines to instability due to the presence of ice accretions. The paper presents results obtained with two different numerical approaches used to estimate galloping amplitudes on overhead transmission lines. The benchmark case relates to a 400 m single span of four-bundled conductor. A triangular shape of ice, whose aerodynamic coefficients are known by previous experiments in the wind tunnel, is considered as applied to the conductors. The two numerical models described in the paper are based on significantly different approaches even though both use the quasi-steady theory (QST) to reproduce the motion dependent aerodynamic forces. The first model relies on a full non-linear FE model running in time domain, while the second is mainly based on the energy balance method. Despite the different approach in modelling, the estimation of galloping amplitudes considering different ice shape configurations matches with a maximum error of 11 % in the estimation of the maximum vertical amplitude reached at midspan. Consequently, the two approaches can be employed to optimize the configuration of anti-galloping devices on a transmission line. Moreover, this work can represent a robust benchmark for assessing the validity of newly developed galloping models.

1. Introduction

Galloping of transmission overhead lines is a wind-induced vibration phenomenon characterized by large amplitudes at low frequencies related to the first modes of vibration of bundled conductors (Zanelli et al., 2022). Galloping occurs when an ice accretion is present on the conductors. The galloping phenomenon can significantly damage the overhead transmission lines due to possible phase-to-phase flashover and large dynamic loads on the support structures. Indeed, severe damages and failures of conductors and their interconnected equipment have been reported after galloping events (CIGRE International Council on Large Electrical Systems, 2007). Since the impact of the galloping phenomenon is very relevant on the maintenance and life of overhead transmission lines, several numerical models have been developed to study the phenomenon. The first numerical model was developed by Den Hartog (Den Hartog, 1932) in 1932: his mathematical model of the galloping mechanism was based on the one degree of freedom (1-DoF) system. In 1974 Blevins and Iwan presented a two-degree-of-freedom (2-DoF) model (Blevins and Iwan, 1975) to study the galloping phenomenon. In the following years, several contributions to improve the numerical models have been introduced by different researchers. In 1998 Chabart and Lilien measured the aerodynamic coefficients of a single conductor covered with an artificial ice shape and implemented a numerical galloping model of a short straight segment of an iced single conductor (Chabart and Lilien, 1998). The measured aerodynamic coefficients were then used in (Keutgen and Lilien, 2000) to prove the validity of a finite element model.

It has been pointed out that galloping in transmission lines is more likely to occur in multi-bundled conductor lines than in single-conductor one (The Institute of Electrical Engineers of Japan, 2001). Matsumiya et al. have conducted many studies on galloping in four-conductor bundled lines through field observations ((Matsumiya et al., 2022a), (Taruishi and Matsumiya, 2023)), and wind tunnel tests ((Matsumiya et al., 2011), (Matsumiya et al., 2018) and (Matsumiya et al., 2022b)). They observed that actual galloping involves a coupled vertical-horizontal-torsional three-degrees-of-freedom (3-DoF)

* Corresponding author.
E-mail address: federico.zanelli@polimi.it (F. Zanelli).

https://doi.org/10.1016/j.jweia.2025.106285
Received 14 July 2025; Accepted 13 November 2025
Available online 19 November 2025
0167-6105/© 2025 The Authors. Published by Elsevier Ltd. This is an open access article under the CC BY-NC-ND license (http://creativecommons.org/licenses/by-nc-nd/4.0/).

oscillation. They also studied the steady and unsteady aerodynamic characteristics of ice-accreted four-bundled conductors, including the dependence on ice accretion shapes and the wake effect between sub-conductors. In particular, Matsumiya et al. (2018) developed an experimental technique for the elastic support of a sectional model of a wind tunnel. This technique can be used to physically simulate 3-DoF galloping with large amplitudes. The applicability of quasi-steady aerodynamic force modelling for four-bundled conductors was then discussed by comparing the response amplitudes of the time history analysis with those of the wind response measurement tests. In conclusion, although it is necessary to model the quasi-steady aerodynamic forces for each individual sub-conductor rather than for all four conductors together, it was found that the quasi-steady aerodynamic force modelling can predict the response with sufficient accuracy.

Nowadays, most numerical models used to estimate the galloping vibration amplitudes are based on the finite element (FE) approach ((Keutgen and Lilien, 2000) (Mou et al., 2020)) or on simplified methods ((Liu et al., 2021)). However, the number of available models is still limited, and they are mainly confined to a research level, providing limited support to the engineering practise. In this framework there is still a lack of validation of the different numerical approaches with respect to experimental data collected from operative transmission lines. Moreover, the complex combination of mechanical, aerodynamical and meteorological aspects still makes it an open research topic, and there are margins for improvement in modelling the phenomenon (Gonzalez-Fernandez et al., 2025). As an example, technical literature reports the value of aerodynamics coefficients for different ice shapes obtained through wind tunnel tests (Chabart and Lilien, 1998) (Lu et al., 2019) (EPRI, 2009); nonetheless the understanding on what type of ice or snow accretion can lead to galloping instability in the case of both single and bundle conductors needs still to be investigated.

In this paper, a comparative analysis of numerical results obtained using two different numerical models based on significantly different approaches is reported. The first numerical model, developed by the Central Research Institute of Electric Power Industry (CRIEPI), relies on a full non-linear FE model running in the time domain. The second one, developed by Politecnico di Milano (POLIMI), is mainly based on the energy balance method.

The initial stage in the benchmark targets a simple analytical model for a single span of four bundled-conductor lines without modelling insulators. In Section 2, the two numerical approaches will be described in detail, while the benchmark case will be presented in Section 3. Finally, the results of the comparison will be presented and discussed in Section 4.

It is worth noting that the numerical approach to reproduce the galloping phenomenon, if suitably verified, can be extremely useful to optimize the different devices used for galloping mitigation, such as detuning pendulums or interphase spacers.

2. The numerical approaches used for the benchmark

The numerical approaches considered in this paper for the estimation of galloping vibrations are developed by CRIEPI and POLIMI. For the definition of the aerodynamic forces on the iced conductors, both the numerical models consider the quasi-steady theory (QST). The QST is widely used to reproduce the aerodynamic forces on a body of any shape moving with respect to the incoming wind when the reduced velocity V_R is greater than 20–30 (Diana et al., 2004). The reduced velocity is defined as:

$$V_R = \frac{V}{fD} \tag{1}$$

where V is the wind speed, f is the frequency of the body motion and D is a typical dimension of the body (i.e., for cylindrical bodies, as conductors, the parameter D corresponds to the diameter). In general, the reduced velocity V_R can be interpreted as the ratio between the period associated to the body vibration (T = 1/f) and the time B/V needed by the fluid particle to move through the conductor diameter D. A high reduced velocity means that the time needed by a particle to cross the body is very small compared to the period of oscillation of the body: thus, aerodynamic forces are in small amount influenced by the motion frequency and aerodynamic coefficients obtained through static tests can then be employed. The galloping phenomenon typically occurs for high values of wind speeds (generally greater than 10 m/s) when the frequency of body motion is generally lower than 1 Hz (EPRI, 2009). This means that, considering a typical conductor diameter D in the order of 30 mm, the reduced velocity V_R for galloping is greater than 30 and this fact widely justifies the use of the QST to reproduce the aerodynamic forces in case of galloping phenomenon.

According to the QST, the aerodynamic forces in the numerical models used to estimate galloping vibrations are defined based on the aerodynamic coefficients identified through static tests in wind tunnel for the conductors with ice but considering the effect of the body motion by computing the relative velocity of the wind with respect to the moving body (Argentini et al., 2022).

In the following, the two approaches are described in detail.

2.1. The CRIEPI model

To simulate the galloping on overhead transmission lines, CRIEPI has developed a numerical analysis programme based on the FEM analysis method, called 'CAFSS' ((Shimizu et al., 1998) (Shimizu, 2010)). Since the prototype version has been published in 1996, CAFSS has been updated in the perspectives of modelling of aerodynamic forces, considering galloping countermeasures, and user-friendly graphical user interface (GUI) for making FEM models. CAFSS has been used by many electric power companies in Japan. In a typical analysis of overhead transmission lines, each component of the actual structure is modelled as accurately as possible, and the analysis is performed by specifying the physical properties of each component. The geometries and masses of the insulators and spacers in a four-conductor bundle can be considered, and the sub-conductors between the spacers can move independently. The simulation results obtained through CAFSS were verified by comparing with a series of galloping observations conducted at Mogami Test Line in Japan (Shimizu and Sato, 2005). The observation object was one span of a real scale four-conductor bundle with artificial ice of triangular shape. It was clarified that the simulation and observation results showed good agreements if both structural and aerodynamic conditions were obvious.

The structural and aerodynamic models can be constructed using conventional methods that were adopted in simulations using CAFSS. Conductors adopted to overhead power transmission lines generally have several millimetres of the diameter, several hundred metres of the span, and ten or more metres of the sag. As a consequence, it can be stated that the conductors can definitely be considered slender structures and therefore they are generally treated as cable structures, namely, bending stiffness is ignored because its effect is negligible (Henghold and Russell, 1976). Hence, the conductors are typically modelled using two-node cable elements with three translational degrees of freedom and one torsional degree of freedom around the horizontal axis. Other components, such as insulators and spacers, are modelled using two-node beam elements with three translational and torsional degrees of freedom. In this study, the authors focused on the simple four-conductor bundle model consisting of only cable elements. The equation of motion for cable element is written in incremental form as:

$$[m]\Delta\{\ddot{u}\} + [c]\Delta\{\dot{u}\} + [k]\Delta\{u\} = \Delta\{f\} \tag{2}$$

where $[m]$, $[c]$, and $[k]$ are the mass, damping, and stiffness matrices, respectively. Considering the cable element shown in Fig. 1 as an

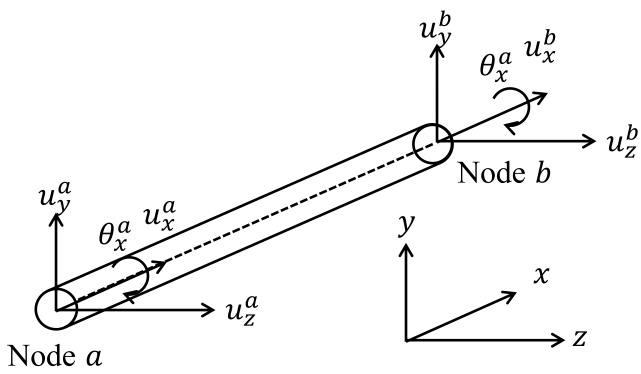

Fig. 1. Definition of cable element.

example, the node displacement vector $\{u\}$ and the nodal force vector $\{f\}$ are defined as

$$\{u\} = \left\{u_x^a\ u_y^a\ u_z^a\ \theta_x^a\ u_x^b\ u_y^b\ u_z^b\ \theta_x^b\right\}, \{f\} = \left\{f_x^a\ f_y^a\ f_z^a\ m_x^a\ f_x^b\ f_y^b\ f_z^b\ m_x^b\right\} \tag{3}$$

To consider geometric non-linearity, the stiffness matrix is defined as:

$$[k] = \frac{1}{l}\begin{bmatrix} EA & 0 & 0 & 0 & -EA & 0 & 0 & 0 \\ 0 & 0 & 0 & 0 & 0 & 0 & 0 & 0 \\ 0 & 0 & 0 & 0 & 0 & 0 & 0 & 0 \\ 0 & 0 & 0 & GJ & 0 & 0 & 0 & -GJ \\ -EA & 0 & 0 & 0 & EA & 0 & 0 & 0 \\ 0 & 0 & 0 & 0 & 0 & 0 & 0 & 0 \\ 0 & 0 & 0 & 0 & 0 & 0 & 0 & 0 \\ 0 & 0 & 0 & -GJ & 0 & 0 & 0 & GJ \end{bmatrix} + \frac{F}{l}\begin{bmatrix} 1 & 0 & 0 & 0 & -1 & 0 & 0 & 0 \\ 0 & 1 & 0 & 0 & 0 & -1 & 0 & 0 \\ 0 & 0 & 1 & 0 & 0 & 0 & -1 & 0 \\ 0 & 0 & 0 & 0 & 0 & 0 & 0 & 0 \\ -1 & 0 & 0 & 0 & 1 & 0 & 0 & 0 \\ 0 & -1 & 0 & 0 & 0 & 1 & 0 & 0 \\ 0 & 0 & -1 & 0 & 0 & 0 & 1 & 0 \\ 0 & 0 & 0 & 0 & 0 & 0 & 0 & 0 \end{bmatrix} \tag{3}$$

The first term is a linear stiffness matrix, where EA is the axial stiffness and GJ is the torsional stiffness. The second term represents the geometric stiffness matrix, where F represents the axial force. Geometric non-linearity is considered by updating the second term at each time step.

In galloping simulations using CAFSS, the aerodynamic forces acting on snow-accreted conductors are typically implemented using a quasi-steady aerodynamic force model. The aerodynamic forces at node a are generated in the y–z plane of the elemental coordinate system by the relative wind velocity v_r^a. Drag force F_D^a, lift force F_L^a, and aerodynamic momentum F_M^a are expressed by:

$$F_D^a = \frac{1}{2}\rho_a d C_D(\alpha_r^a) v_r^{a2} \times \frac{1}{2} l, F_L^a = \frac{1}{2}\rho_a d C_L(\alpha_r^a) v_r^{a2} \times \frac{1}{2} l,\ F_M^a = \frac{1}{2}\rho_a d^2 C_M(\alpha_r^a) v_r^{a2} \times \frac{1}{2} l \tag{4}$$

$$v_r^{a^2} = \left(v_y - \dot{u}_y^a\right)^2 + \left(v_z - \dot{u}_z^a\right)^2, \alpha_r^a = \psi^a - \phi_o, \psi^a = \tan^{-1}\left(\frac{v_z - \dot{u}_z^a}{v_y - \dot{u}_y^a}\right) \tag{5}$$

Here, ψ^a is the incident angle, ϕ_o is the initial snow-accretion angle, and α_r^a is the attack angle. ρ_a, d, and l are the air density, element diameter, and element length, respectively. For the drag, lift, and moment coefficients C_D, C_L, and C_M, aerodynamic coefficients of the model snow-accreted conductor measured through wind tunnel tests, are typically used. The aerodynamic forces at node b are written in the same way. Accordingly, the nodal force vector $\{f\}$ is defined as

$$\{f\} = \left\{\begin{matrix} f_x^a \\ f_y^a \\ f_z^a \\ m_x^a \\ f_x^b \\ f_y^b \\ f_z^b \\ m_x^b \end{matrix}\right\} = \left\{\begin{matrix} 0 \\ F_D^a \cos\psi^a - F_L^a \sin\psi^a \\ F_D^a \sin\psi^a + F_L^a \cos\psi^a \\ F_M^a - F_D^a \cos\psi^a s_z + F_D^a \sin\psi^a s_y + F_L^a \cos\psi^a s_y + F_L^a \sin\psi^a s_z \\ 0 \\ F_D^b \cos\psi^b - F_L^b \sin\psi^b \\ F_D^b \sin\psi^b + F_L^b \cos\psi^b \\ F_M^b - F_D^b \cos\psi^b s_z + F_D^b \sin\psi^b s_y + F_L^b \cos\psi^b s_y + F_L^b \sin\psi^b s_z \end{matrix}\right\} \tag{6}$$

This study targets a simple analytical model for a four-conductor bundle line. In (Taruishi and Matsumiya, 2023) the authors pointed out that the quasi-steady aerodynamic forces of a four-conductor bundle during large-amplitude galloping should be formulated independently for each sub-conductor, rather than formulating these forces for the entire bundle. They also clarified that the aerodynamic forces caused by the torsional velocities of entire four-conductor bundle can be formulated using an individual sub-conductor aerodynamic force model, and this factor is important for accurately estimating the response amplitude. However, in FEM analysis, even when four-conductor bundle lines are targeted, their elements are naturally created for each sub-conductor, thus modelling the aerodynamic forces for each sub-conductor, and therefore this concern has been resolved.

As the initial stage in the benchmark, the simple analytical model of a four-conductor bundle line is composed only of the wires, without modelling insulators or spacers as described in Section 3. This model does not allow independent movement of the sub-conductors between the spacers; the spacing between the four individual sub-conductors remains constant. Therefore, multipoint constraint conditions were applied to the sub-conductors at the same axial location along the span. To apply multipoint constraint conditions, another original programme specialised for research purposes ((Matsumiya et al., 2021)) was used. Although structural modelling based on FEM and aerodynamic force modelling based on quasi-steady theory are the same as in CAFSS, there are no user-oriented features such as a GUI; both non-linear and linear models for structural and aerodynamic forces can be used in this programme. In addition to static and dynamic analyses (time history response analysis), eigenvalue analysis and complex eigenvalue analysis (linear instability analysis) can be performed.

Finally, in Table 1 the parameters of the time-history response analysis in the CRIEPI model are summarised. In particular, for the benchmark simulations discussed in this paper the time series of the responses were analysed over 800 s, and the mean values and peak-to-peak amplitudes were calculated.

2.2. The POLIMI model

The POLIMI numerical model for the calculation of maximum

Table 1
Time-domain finite element analysis parameters in the CRIEPI model.

Integration method	Newmark β method ($\beta = 1/4, \gamma = 1/2$)
Iterative method	Newton–Raphson method
Integration time step	0.001 s
Output time step	0.05 s
Analysis period	800 s

vibration amplitudes of bundled conductors due to ice galloping phenomenon is based on a numerical procedure structured in three steps (Diana et al., 2021). The first step consists in calculating the static configuration of the bundled conductors as a function of wind speed and weight of ice on the conductors by using a Finite Element Model (FEM). An iterative algorithm is adopted to compute the equilibrium configuration where the tensile preload of finite elements changes along the span due to the effect of the static load. This first step is very similar to the one adopted in CRIEPI model. In the FEM creation stage, it is possible to consider the structural characteristics of the bundled conductors: cable elements with three translational degrees of freedom and one torsional degree of freedom for each node are used for each conductor (Fig. 2). A lumped-parameter model is adopted to describe the effect of spacers that may be introduced in generic positions along the span. Under typical galloping conditions, relative displacements among sub-conductors are small compared to the whole bundled conductor motion. For this reason, the main contribution of spacers taken into account in the model is related to the inertia added by considering the lumped-parameter model. Moreover, for the same reason, an equivalent super-conductor that represents the motion of the bundled conductor is considered in the numerical procedure.

The structural matrices of the super-conductor are defined considering rigid kinematic relationships between the four degrees-of-freedom (DoF) of each node of the conductors, modelled by string elements, and the six DoF of the super-conductor. As in the CRIEPI model, the six DoF describe the displacements of the bundle axis and the rotations of each bundle section. The kinematic relationships between the DoF of the string element nodes and the DoF of the super-conductor nodes are defined by the rectangular matrix (8x12) $[\Lambda_{jk}]$, being j the index related to the finite elements along the axis of the bundled conductor and k the index related to the sub-conductors of bundled conductor:

$$\underline{x}_{S,jk} = [\Lambda_{jk}]\underline{x}_{B,j} \quad j = 1, N \quad k = 1, Nc \tag{7}$$

In equation (7) $\underline{x}_{S,jk}$ and $\underline{x}_{B,j}$ are the vectors that collect, respectively, the eight DoF of the string element, and the twelve DoF of the beams super-conductor while N and Nc are respectively the number of elements along the span (i.e. N is equal to the ratio between the span length and the finite element length) and the number of sub-conductor (in the analysed case $Nc = 4$).

Through well-known transform matrices, the super-conductor structural matrices are easily defined:

$$\begin{cases} [\mathrm{M}_{B,j}] = \sum_{k=1}^{Nc}\left([\Lambda_{jk}]^T[\mathrm{M}_{S,jk}][\Lambda_{jk}]\right) \\ [\mathrm{K}_{B,j}] = \sum_{k=1}^{Nc}\left([\Lambda_{jk}]^T[\mathrm{K}_{S,jk}][\Lambda_{jk}]\right) \end{cases} \quad j = 1, N \tag{8}$$

The second step of the procedure is the computation of the natural frequencies and the vibration modes of the bundled conductor around the static configuration defined in the step 1, which considers the horizontal and vertical deflection of the bundled conductors due to ice weight and aerodynamic forces related to the average wind speed. The considered natural frequencies are the ones in the typical frequency range of galloping, i.e. below 1 Hz.

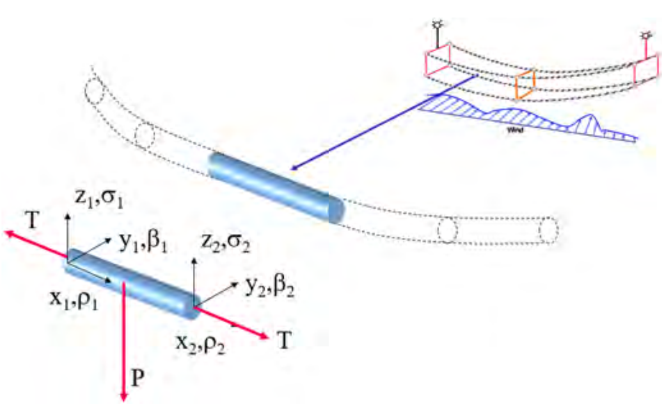

Fig. 2. Finite Element Model: schematization of conductors.

Applying a modal analysis approach and defining $\mathbf{q}$ the vector of modal coordinates, the aerodynamic forces and moments can be conveniently collected in a unique vector $\boldsymbol{F_a}(\boldsymbol{q}, \dot{\boldsymbol{q}}, t)$. The virtual work of aerodynamic forces can thus be expressed as:

$$\delta L = \boldsymbol{F_a}(\boldsymbol{q}, \dot{\boldsymbol{q}}, t)[\boldsymbol{\Phi}]\delta\boldsymbol{q} = \boldsymbol{Q_a}(\boldsymbol{q}, \dot{\boldsymbol{q}}, t)^T\delta\boldsymbol{q} \tag{9}$$

where $[\boldsymbol{\Phi}]$ is the matrix of mode shapes and the explicit dependence on time is due to the time histories of wind speeds acting on different sections of the bundle. The equations of motion of the super-conductor are eventually assembled as follows:

$$[\boldsymbol{M}]\ddot{\boldsymbol{q}} + [\mathbf{C}]\dot{\boldsymbol{q}} + [\boldsymbol{K}]\boldsymbol{q} = \boldsymbol{Q_a}(\boldsymbol{q}, \dot{\boldsymbol{q}}, t) \tag{10}$$

where **[M]**, **[C]** and **[K]** are diagonal matrices containing mode mass, damping and stiffness of each eigenmode. The damping matrix is obtained as a linear combination of mass and stiffness matrices (Rayleigh model).

The third step consists in linearizing the numerical model, including the aerodynamic forces, around the static configuration defined in step 1, and computing the eigenvalues and eigenmodes for different wind speeds including the aeroelastic effects. The eigenmodes whose eigenvalues have a positive real part identify the unstable motions. The process identifies the onset of unstable modes for different wind speeds. Eigenmodes are expressed in terms of combination of the modal coordinates introduced in the step 2. Even though such modal coordinates essentially represent n-lobe motions in the vertical/horizontal plane or n-lobe rotations, when aeroelastic effects are introduced, they combine. In this way both 1-dof instability or 2-dof instability (flutter instability) are highlighted.

Each unstable mode "m" is therefore characterized by a circular frequency ω_m and by an eigenmode collecting the complex gains of mode-shapes introduced in step 2. The combination of the mode-shapes allows describing the unstable galloping motion. To determine the oscillation amplitudes of the unstable mode, the eigenvectors are multiplied by a real amplification factor γ. Amplitudes of the limit cycles are associated with the equilibrium between energies introduced and removed from the system. Therefore, γ can be identified by minimizing the difference between the energy introduced by the aerodynamic forces and the energy adsorbed with internal damping in one oscillation cycle. Being T_m the time period of the oscillation obtained as $2\pi/\omega_m$, this means:

$$E = \int_{T_m}\dot{\boldsymbol{q}}^T\boldsymbol{Q_a}(\boldsymbol{q}, \dot{\boldsymbol{q}})dt + \int_{T_m} -\dot{\boldsymbol{q}}^T[\boldsymbol{C}]\dot{\boldsymbol{q}}dt = min \tag{11}$$

Equation (11) is solved iteratively through a minimization algorithm. It must be pointed out that the method considers the aerodynamic force non-linearity and, if available, also the structural damping non-linearity, both related to the amplitude of the motion.

3. The benchmark case

3.1. Structural conditions

As the initial stage in the benchmark, the simple analytical model of a four-conductor bundle line is composed only of the wires, without modelling insulators, as represented in Fig. 3. The main features of the conductors and the span are collected in Table 2. The extremities of conductors are clamped to the ground. This simple configuration avoids introducing differences in the modelling of boundary conditions. Furthermore, this model does not allow independent movement of the

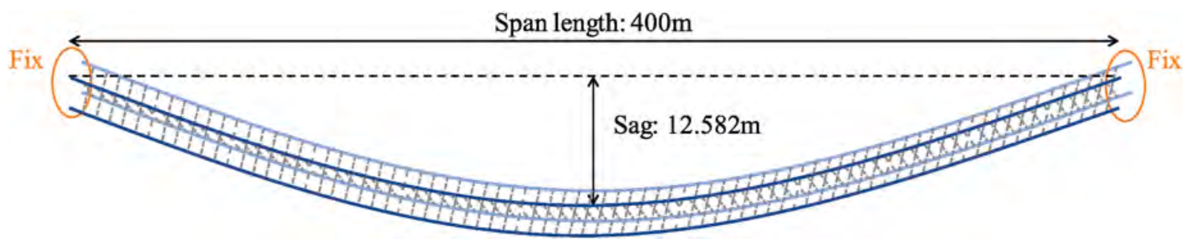

Fig. 3. Representation of the bundle considered for the benchmark activity.

Table 2
Main properties of the bundle selected for the benchmark case.

Conductor properties		
Conductor type	–	ACSR
Cross-sectional area	m^2	0.000481
Representative diameter	mm	28.5
Polar moment of inertia of area	m^4	3.894E-08
Modulus of rigidity	N/m^2	4029751541
Modulus of longitudinal elasticity	N/m^2	81983594000
Mass density	kg/m^3	3479.617
Span Properties		
Span length	m	400
Length of one element (conductor)	m	5
Initial sag	m	12.583
Initial tension	N	26094
Subconductor separation	m	0.4

sub-conductors between the spacers; the spacing between the four individual sub-conductors remains constant.

In the CRIEPI model, the multipoint constraint conditions were applied to the sub-conductors at the same axial location along the span. Briefly, virtual spacers were placed at all 80 nodes in the span of the model shown in Fig. 3 to constrain the independent movement of the sub-conductors. Consequently, a four-conductor bundle line is treated equivalently to a single-conductor line, which is called an 'equivalent single-conductor model'. The response of the overhead transmission line is expressed as a six-DoF motion of the centre of a four-bundled conductor. However, vertical and horizontal displacements and torsion angles were the focus of this study.

In the POLIMI model, as reported in the previous section, the structural matrices of the super-conductor are defined considering rigid kinematic relationships between the four-DoF of each node of the sub-conductors, modelled by string elements, and the six-DoF of the super-conductor.

The damping for the FE models of the bundled conductor were introduced according to the Rayleigh model: the damping matrix $[\mathbf{C}]$ is defined as $[\mathbf{C}] = \alpha[\mathbf{M}] + \beta[\mathbf{K}]$, being $[\mathbf{M}]$ and $[\mathbf{K}]$ respectively the mass and stiffness matrices. This relationship allows to define the nondimensional damping ratio h_i for a natural circular frequency ω_i as:

$$h_i = \frac{\alpha}{2\omega_i} + \frac{\beta\omega_i}{2} \tag{12}$$

The values of parameters α and β are obtained minimizing the root square error between equation (12) and the value of nondimensional damping ratio at different values of natural frequencies, as reported in Table 3. The damping values were estimated based on field test results (Taruishi et al., 2021).

Table 3
Main properties of the bundle selected for the benchmark case.

Rayleigh damping		
frequency 1	Hz	0.15606022
frequency 2	Hz	2
damping ratio for 1	–	0.005
damping ratio for 2	–	0.005

In this study, the results are presented according to the definitions of displacements and angles as shown in Fig. 4, although a right-hand coordinate system is adopted in the FEM analysis.

3.2. *Ice shape parameters and aerodynamic characteristics*

For the benchmark case, the considered shape of ice is triangular, as shown in Fig. 5 (a): the distance from the vertex of the triangle and the surface of the conductor is equal to its radius. The aerodynamic coefficients of the conductors plus this type of ice shape were characterized by Matsumiya et al. (2018)) in the wind tunnel and their diagrams are reported in Fig. 5 (b). In the case of a four-bundled conductor, the aerodynamic forces acting on the downstream sub-conductors can be influenced by the wake generated by the upstream sub-conductors. This behaviour differs from that observed in single-conductor lines. For the main purpose of benchmarking related to galloping, this study assumes that the aerodynamic force coefficients acting on all sub-conductors are the same. However, the wake effect for high angle of attack is low and it can be neglected.

Additionally, the analyses were conducted in two cases of ice accretion angles: one with an upward tilt of 10° (+10°) from the horizontal direction and another with a downward tilt of 10° (−10°).

Fig. 6 (a) shows the orientation of ice formations for the −10° case. The shape of the ice is the same seen in Fig. 5 (a), but the apex of ice accretions points downward; the chord of the profile presents an inclination of −10° with respect to the horizontal direction. This feature confers a downforce effect to the profile. As shown in Fig. 6 (b), an angle of attack of the wind speed (AoA) of 0° corresponds to a negative lift coefficient for the single conductor. In a similar way, the moment coefficient is negative indicating that an anticlockwise moment is developed.

Fig. 7 (a) shows the orientation of ice formations for the 10° case. In this condition, the chord of the profile is pointing upward, i.e. it is inclined by 10° clockwise, with respect to the horizonal direction. The profile is thus able to generate a lift force. As shown in Fig. 7 (b), an AoA

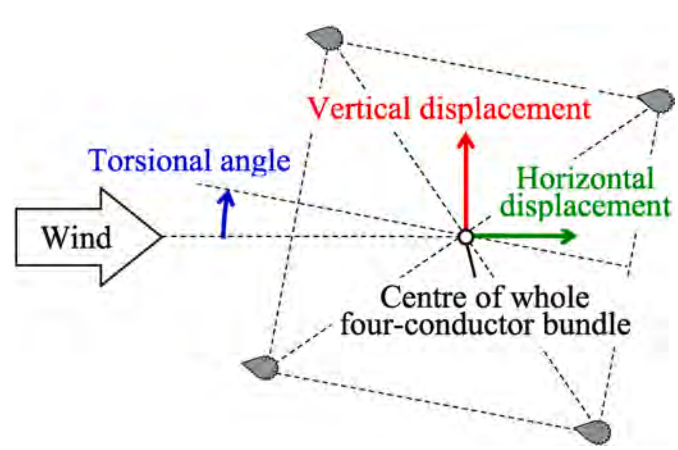

Fig. 4. Convention for displacement and angles.

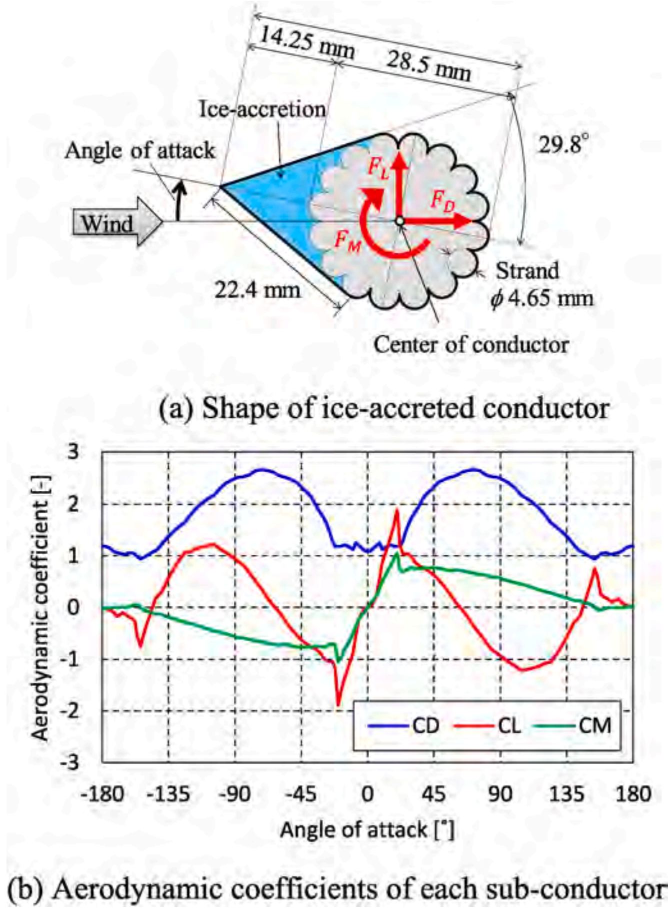

Fig. 5. Considered ice shape (a) and related aerodynamic coefficients (b).

of 0° corresponds to a positive lift coefficient. In a similar way, the moment coefficient is positive, so a clockwise moment is developed.

In Figs. 6(b) and 7(b), the steady aerodynamic force coefficients for the entire four-conductor bundle were simply calculated from the steady aerodynamic force coefficients of each sub-conductor ((Matsumiya et al., 2011)). It must be considered that the four-conductor bundle is subject to vertical, horizontal and torsional motion and for the computation of the aerodynamic forces using QST the velocities of the four sub-conductors are all different due to the torsional motion of the bundle (Matsumiya et al., 2018) (Matsumiya et al., 2022b). For this reason, the aerodynamic forces are different for each sub-conductor.

The air density was assumed equal to 1.275 kg/m^3. The task of the benchmark was to compare the numerical results of the models by CRIEPI and POLIMI, with particular reference to prediction of galloping oscillation amplitudes for wind speeds up to 20 m/s.

4. Comparison of results obtained with the two numerical approaches

In this section, the main results obtained through the two models are compared. The analysis takes into account as a first step the computation of eigenfrequencies and eigenmodes of the structure obtained around the static equilibrium position without wind. The second step is represented by the static configuration assumed by the cable under the effect of mean wind speed. Subsequently, a linearization around the static configuration is performed to compute eigenmodes and obtaining a comparison in terms of frequencies and damping. In the end, maximum galloping amplitudes are obtained as a function of the wind speed. All results are reported for both type of ice accretion considered (−10° and +10° cases).

4.1. Eigenfrequencies and eigenmodes without wind

The first comparison between CRIEPI model and POLIMI model is performed in terms of eigenmodes and eigenfrequencies of the overhead transmission line structural model. Table 4 lists the eigenmodes identified by the two codes, sorted in terms of increasing frequency. The computation is performed at zero wind speed, that is around the static equilibrium position due to weight. The purpose of the comparison is to evaluate the consistency in terms of linear response of the structural models, without including the effect of wind.

Columns 3 and 4 of Table 4 report the eigenfrequencies of the modes described in column 2 obtained with the two numerical models. The comparison reveals a good match in terms of eigenfrequencies. Also, the order of the modes is the same for both codes. Therefore, the structural models of the two codes seem consistent, at least in a linear analysis.

As an example, in Fig. 8 the first nine eigenmodes obtained with the analysis carried out by the CRIEPI model are shown. As can be seen, due to the sag in the transmission lines (i.e. catenary effect), the vertical one-loop mode (6th mode in Fig. 8) is deformed, resulting in a higher frequency. Therefore, the frequency of the vertical symmetric first mode is higher than that of the asymmetric first mode. Similarly, it can be observed that the frequency of the torsional symmetric first mode tends to be higher than that of the asymmetric first mode. Equal results are obtained with the analysis carried out by the POLIMI model.

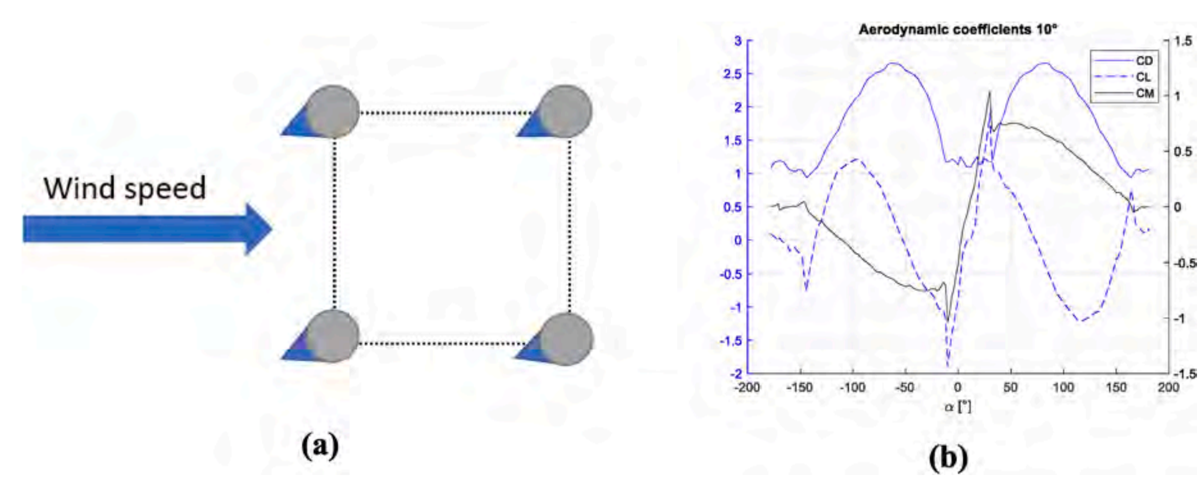

Fig. 6. Ice accretion configuration for the −10° case (a) and corresponding static aerodynamic coefficients for entire four-bundled conductor (b).

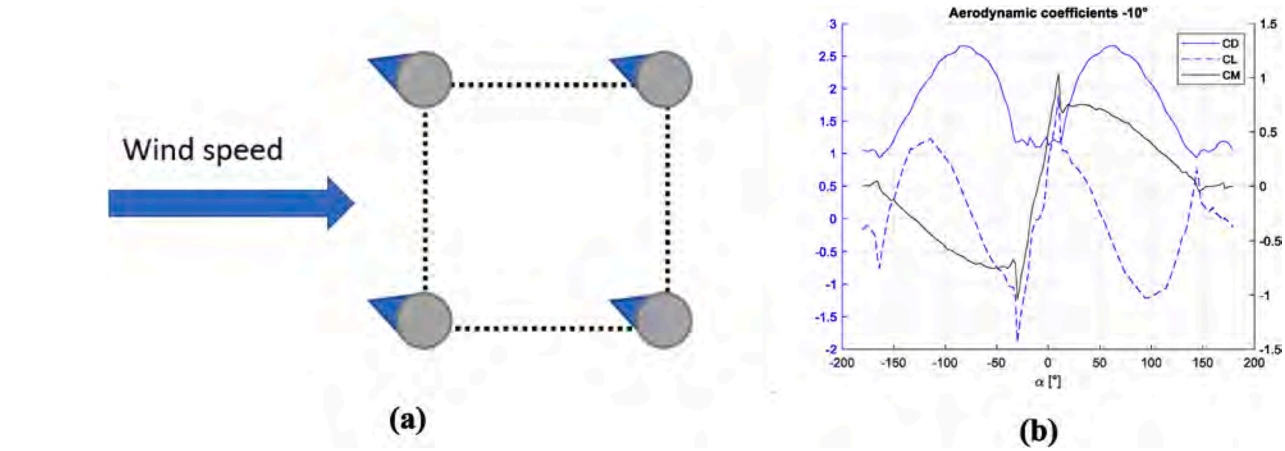

Fig. 7. Ice accretion configuration for the +10° case (a) and corresponding static aerodynamic coefficients for entire four-bundled conductor (b).

Table 4
Comparison of the eigenmodes estimated with the two models.

Mode	Description	CRIEPI	POLIMI
1	1-loop horizontal	0.156 Hz	0.153 Hz
2	2- loop vertical	0.310 Hz	0.304 Hz
3	2-loop horizontal	0.311 Hz	0.305 Hz
4	2-loop torsional	0.321 Hz	0.316 Hz
5	1-loop torsional	0.333 Hz	0.338 Hz
6	1-loop vertical	0.399 Hz	0.399 Hz
7	3-loop horizontal	0.467 Hz	0.458 Hz
8	3-loop torsional	0.500 Hz	0.495 Hz
9	3-loop vertical	0.531 Hz	0.535 Hz
10	4-loop vertical	0.621 Hz	0.611 Hz
11	4-loop horizontal	0.622 Hz	0.612 Hz
12	4-loop torsional	0.644 Hz	0.633 Hz

4.2. Analysis with −10° ice shape profile

4.2.1. Static configuration with wind

The CRIEPI and the POLIMI models were compared in terms of static configuration due to the mean wind speed. Firstly, Fig. 9 shows examples of the deflection of the conductor in the span, i.e. the static equilibrium position under different wind speeds, obtained by the CRIEPI model. In Fig. 10 the same static positions of the bundle as a function of the wind speed are reported for the CRIEPI and POLIMI models at ¼ and ½ of the span. The red and yellow lines represent the vertical displacement of at ½ span and ¼ span respectively; the left scale allows reading the amplitude in meters. The green lines represent the horizontal displacement at ½ span (dark green) and ¼ span (light green). The blue lines refer to the rotation at ½ span (blue line) and ¼ span (cyan line); in this case the amplitude in degrees is reported on the right scale.

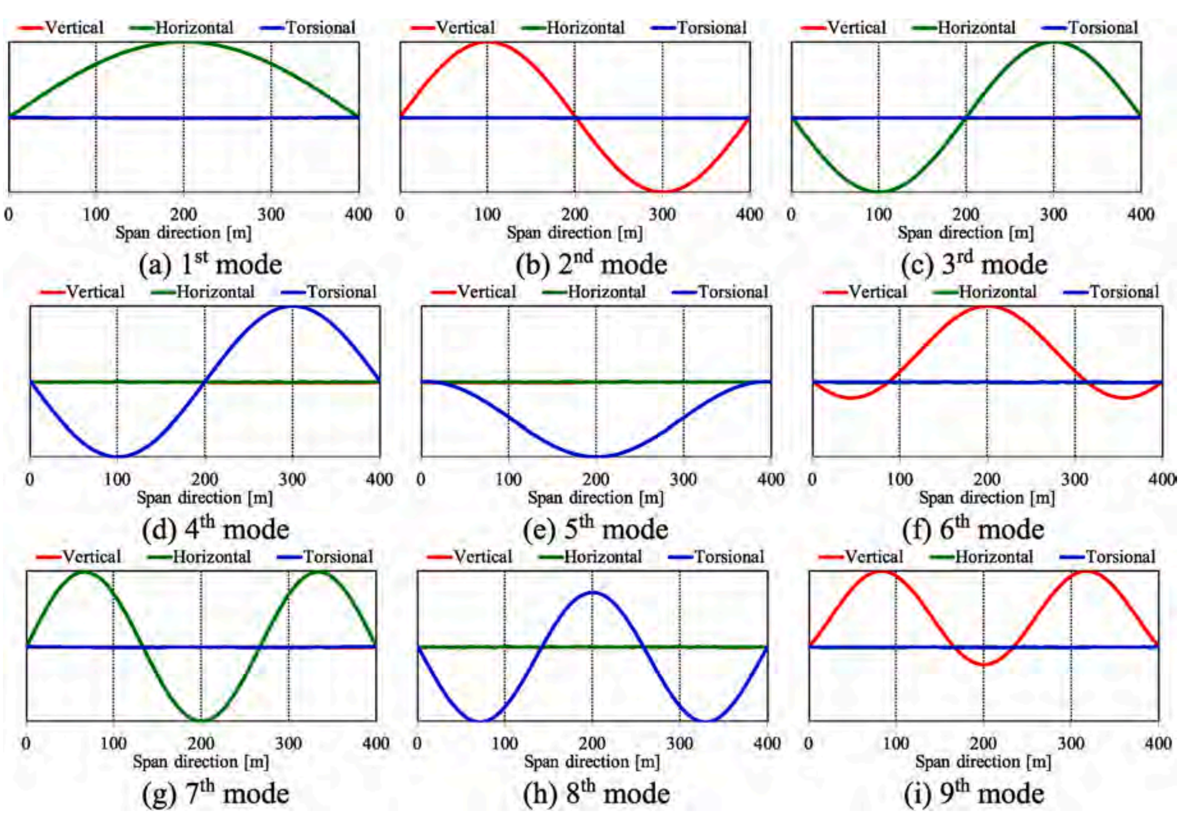

Fig. 8. Shape of eigenmodes without wind (CRIEPI code).

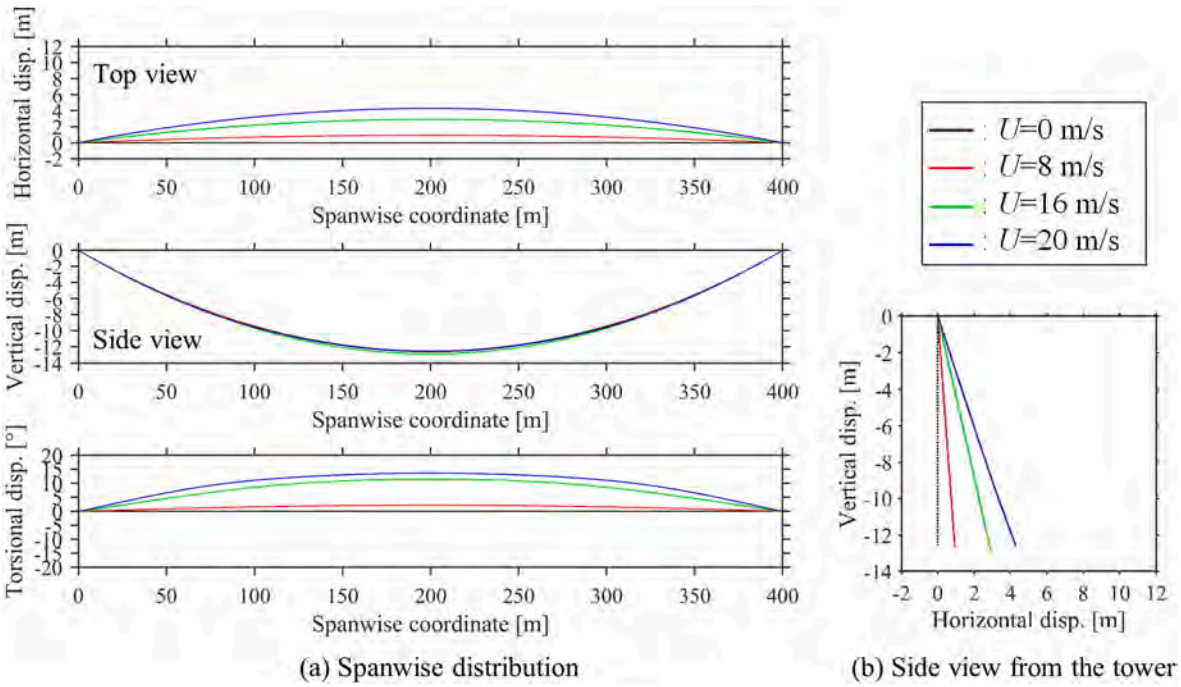

Fig. 9. Bundle static configuration as a function of wind speed (CRIEPI model) for the case of ice shape profile of -10°.

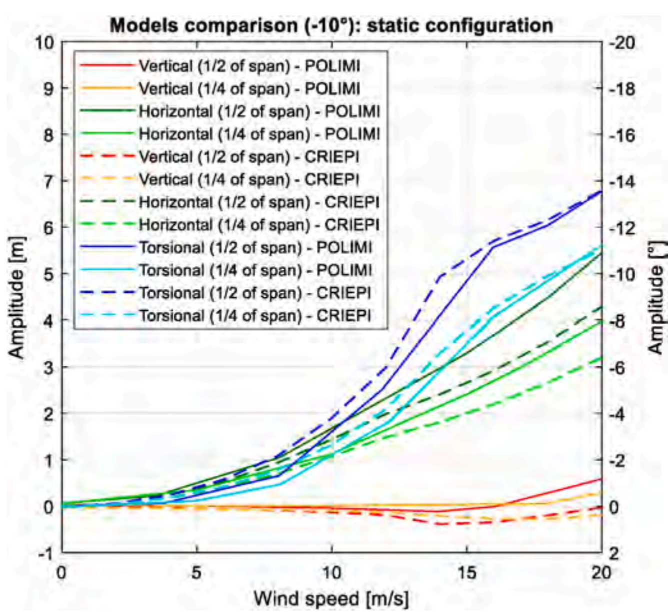

Fig. 10. 10° case, models comparison in terms of static configuration due to constant wind speed (continuous lines: POLIMI results; dashed lines: CRIEPI results).

The two codes predict similar displacements along vertical and horizonal directions. Also, the rotation that determines the angle of attack for different speeds looks almost identical. Considering the midspan, the vertical displacement predicted by CRIEPI model at 20 m/s is almost null. A similar output is provided by POLIMI model. The physical reason behind this result is related to the aerodynamic downforce produced by the orientation of the ice formations. The maximum horizontal displacement is slightly above 4 m for CRIEPI model and above 5 m for POLIMI model. Both the models estimate a maximum rotation of nearly -14° at midspan. Summarising, it is possible to state that the non-linear response of the two models subjected to static effect of wind can be considered consistent, although the two FE approaches are characterized by some differences in the modelling.

4.2.2. Linear analysis

A second step to compare the results was performed computing eigenmodes through the linearization of the aeroelastic model around the static configuration. Actually, this is one of the steps (step 2) adopted by the POLIMI model to estimate galloping amplitudes. Fig. 11 reports the variation of eigenfrequencies of the different vibration modes as a function of wind speed, obtained by eigenvalue analysis. In Fig. 12 the damping ratios, being the ratio between the imaginary part and real part of the computed eigenvalues, are reported as a function of wind speed. Due to the configuration of ice accretion (-10°), the bundle is subjected to a downforce. This effect increases the tensile load with respect to the nominal value. For this reason, eigenfrequencies increase with increasing wind speed. The shapes of the eigenmodes also change from the no-wind conditions shown in Fig. 8 due to the fact that the wind causes variations in the plane where the transmission lines are located, as shown in Fig. 9b. Fig. 11 displays the eigenfrequencies obtained by the CRIEPI model on the left, while the ones on the right refer to the POLIMI model. Both the models predict a similar result for the increase of eigenfrequencies with mean wind speed.

Fig. 12 shows the damping ratios of the complex eigenvalues. Again, CRIEPI results are collected in the left graph. Both the models produce very similar values of the damping ratio. Therefore, the linear analysis highlights instability above this speed.

The damping ratio as a function of wind speed represents a very important parameter because when it assumes a negative value, it is possible to identify the wind speed value at which the instability can occurs is possible. Greater the negative value of the damping ratio, greater is the energy introduced by the aeroelastic forces and more difficult is to control the instability. The eigenmodes related to the negative damping ratios have a different shape in respect to the modes computed without wind effect reported in Fig. 8, and they are in general a combination of vertical, horizontal and torsional modes computed without wind. In the numerical model of POLIMI, for each unstable mode the energy method is applied. The amplitudes of vibration are computed with a balance between the energy introduced by the wind

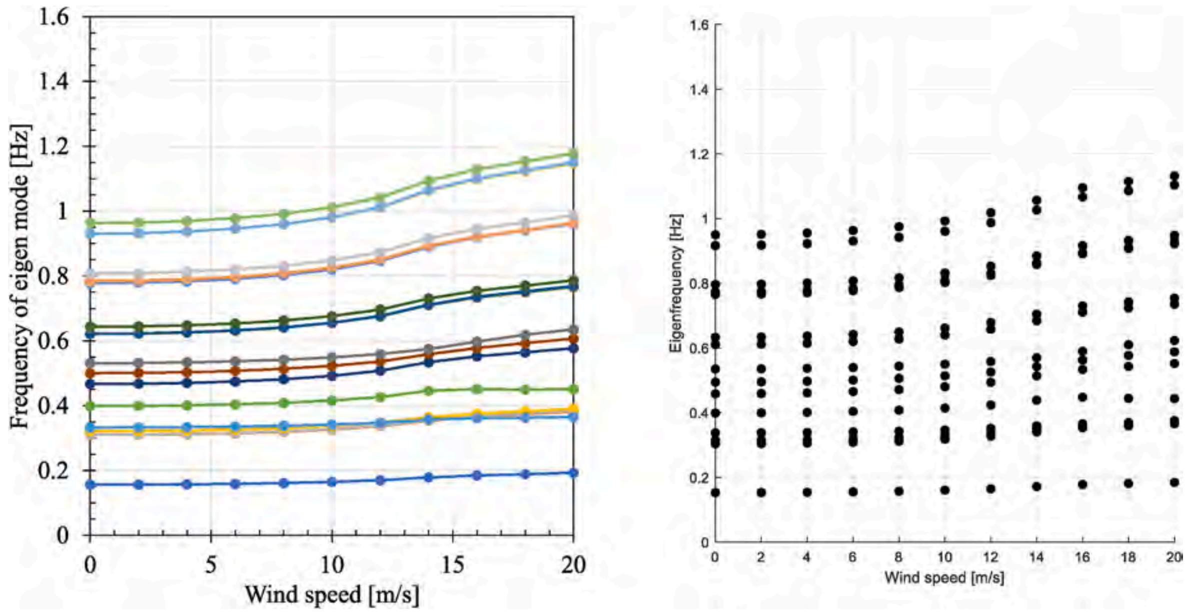

Fig. 11. 10° case, eigenfrequencies VS wind speed: CRIEPI model (left), POLIMI model (right).

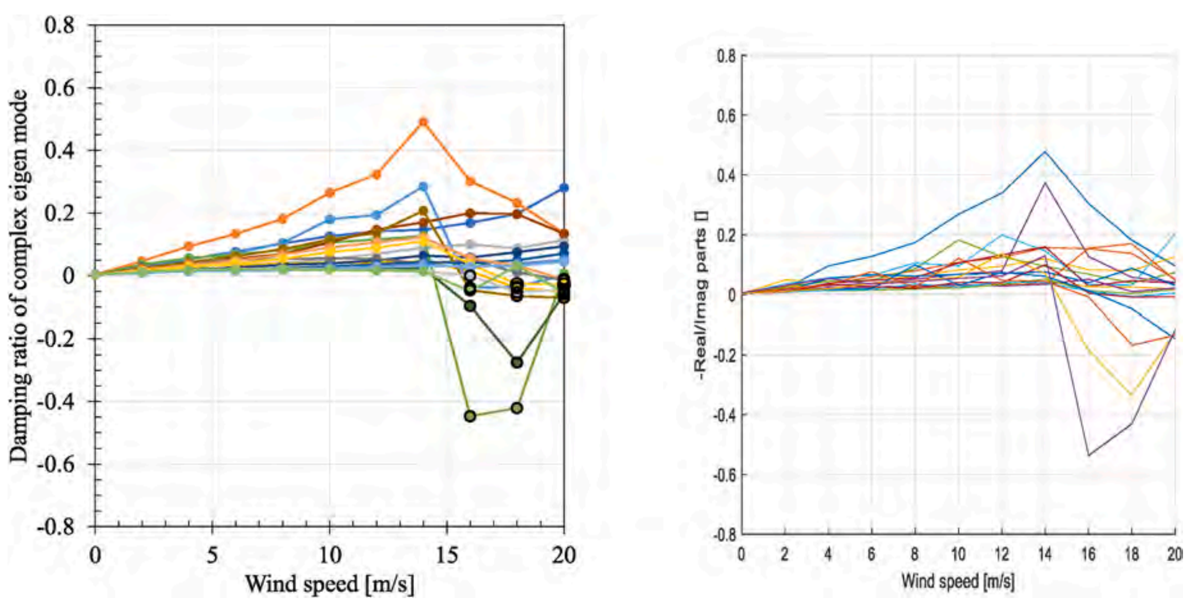

Fig. 12. 10° case, damping ratio of complex eigenmodes VS wind speed: CRIEPI model (left), POLIMI model (right).

and the one dissipated by the system taking into account the non-linearities of the aeroelastic forces. In the CRIEPI model no assumptions are made on the modes that become unstable and the amplitudes of vibration are obtained as peak values of the motion time histories.

4.2.3. Prediction of galloping amplitudes

The last comparison between the two models is in terms of predicted galloping amplitudes. The CRIEPI model uses time-domain simulations to obtain this result. The POLIMI model relies on the energy method for estimating the limit cycle as a result of equilibrium between introduced and dissipated energy. Looking at Fig. 13, the CRIEPI model predicts galloping for wind speeds higher than 14 m/s with amplitudes generally increasing with wind speed. In particular, the maximum vertical displacement (peak-to-peak) is recorded at midspan and is in the order of 2 m. The horizontal vibration is less significant: the peak-to-peak at midspan reaches 0.5 m. As last, the rotation amplitude is in the order of 10°.

Considering Polimi results, reported as continuous lines, again galloping is expected to occur for wind speeds higher than 14 m/s. The increase of wind speed is associated with larger amplitudes. The peak-to-peak oscillation along the vertical direction is slightly below 2 m for a wind speed of 20 m/s. This result is perfectly consistent with CRIEPI model. The same can be said for the horizontal oscillation (0.5 m peak-to-peak) and for the rotation (almost 10° peak-to-peak). The comparison between the two models can therefore be considered fully satisfying, as highlighted by values reported in Table 5 The error in the estimation of the maximum vertical galloping amplitude is approximately 11 %.

4.3. Analysis with +10° ice shape profile

4.3.1. Static configuration

The same analyses by using both numerical models were carried out

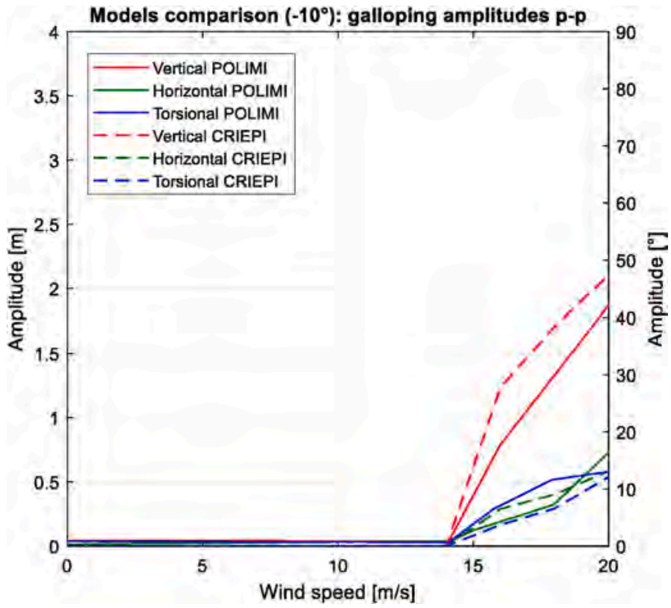

Fig. 13. 10° case, models comparison in terms of galloping amplitudes VS wind speed (continuous lines: POLIMI results; dashed lines: CRIEPI results).

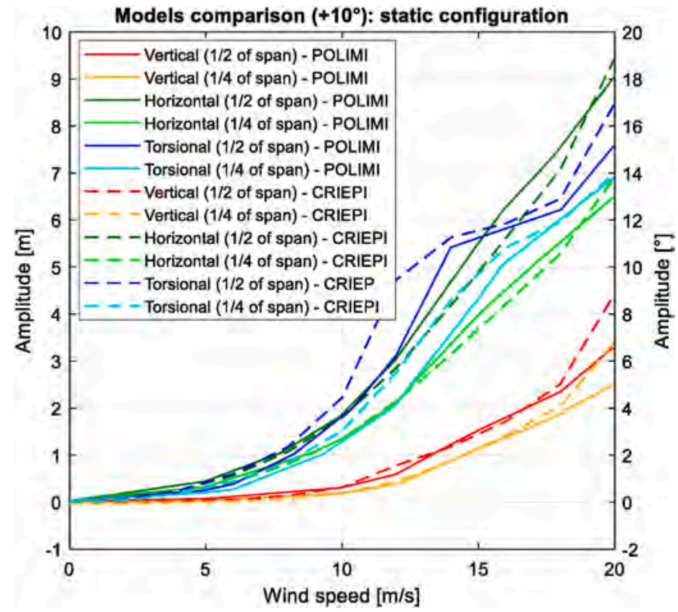

Fig. 14. +10° case, models comparison in terms of static configuration due to constant wind speed (continuous lines: POLIMI results; dashed lines: CRIEPI results).

Table 5
Comparison of the galloping amplitudes estimated at 20 m/s by the two models and relative errors.

Ice shape	Model	Vertical [m]	Horizontal [m]	Torsional [°]
−10°	CRIEPI	2.11	0.58	12.03
	Polimi	1.88	0.73	12.98
	Error [%]	+11 %	−26 %	−8 %

considering the ice accretion angle equal to +10°, i.e., an angle opposite to the one considered in the analyses reported in section 4.2. For the comparison of results obtained with the two numerical models the same steps as described in section 4.2 were followed. The first step was the analysis of static configuration results of the transmission line for both models. The results of the comparison between static configurations at positions corresponding to ¼ and ½ of the span are presented in Fig. 14. Overall, the comparison appears satisfactory: both the models predict similar values for the displacements along vertical and horizonal directions. Also, the rotation that determines the AoA for different speeds looks almost identical. Considering the span centre, the vertical displacement predicted by CRIEPI model at 20 m/s is slightly above 4 m, while it is slightly above 3 m for POLIMI model. The maximum horizontal displacement is around 9 m for both the models. CRIEPI model estimates a maximum rotation of 17° against 15° of POLIMI model. Altogether, the nonlinear response of the two models subjected to static effect of wind can be considered consistent. For the sake of completeness, the static equilibrium position of the conductor in the span under different wind speeds, obtained by the CRIEPI model, is reported in Fig. 15.

4.3.2. Linear analysis

The charts of Fig. 16 report the variation of eigenfrequencies as a function of wind speed for both numerical models. Due to the configuration of ice formations, the bundle is now subjected to a lift force. For the analysed ice formation angle, tension decreases with wind speed, causing the reduction of the eigenfrequencies. The graph on the left displays the data obtained by CRIEPI model, while the one on the right refers to POLIMI model. Both models predict a similar trend for the decrease of eigenfrequencies with mean wind speed.

Fig. 17 displays the damping ratios of the eigenvalues. As usual, the left chart refers to CRIEPI results. Both models identify a negative damping ratio for speeds above 12 m/s. Therefore, the linear analysis highlights instability above this speed. Also in this case, the damping ratios of both model reported in Fig. 17 reach negative values of about −0.4 for a wind speed of 15 m/s. This value is an indication of the high energy introduced by this kind of instability. As can be seen many different modes are unstable. In the next section, values reported in figures refer to the peak-to-peak maximum values of amplitudes of motion as a function of wind speed.

4.3.3. Prediction of galloping amplitudes

The last step for comparing the results of the numerical models is related to the predicted galloping amplitudes. The results are reported in Fig. 18: the usual colour code is used. The CRIEPI model predicts galloping for wind speeds above 12 m/s with amplitudes generally increasing with wind speed. The vertical oscillation shows a local maximum for a wind speed of 18 m/s. In particular, the maximum vertical displacement (peak-to-peak) is obtained at midspan and is in the order of 5 m. This value is significantly higher than the one obtained for the −10° case described in section 4.2. Likely, the reason is the lower tension determined by the lift force developed with this configuration of ice accretion. The horizontal vibration is even larger: the peak-to-peak oscillation nearly reaches 6 m at midspan. The rotation amplitude is in the order of 120°, much larger than the −10° case.

Concerning the POLIMI model, galloping is expected to occur for speeds above 12 m/s; the increase of wind speed is associated with larger amplitudes. The peak-to-peak oscillation along the vertical direction is slightly around 5 m for a wind speed of 20 m/s. This result is consistent with CRIEPI model. The peak-to-peak horizontal oscillation is predicted around 4.5 m, lower than the value outputted by CRIEPI model. In a similar way, according to POLIMI model, the rotation amplitude should be slightly above 20°. In this case the two models are consistent in terms of wind speed range for galloping onset and of vertical amplitudes. The two models reasonably agree in terms of horizontal amplitudes, while significant differences appear for torsional amplitudes. The reasons for such discrepancy are under investigation. Nevertheless, the fact that the torsional amplitude predicted by CRIEPI model is higher with respect to the POLIMI one can be explained considering that the latter takes into account for the computation only a

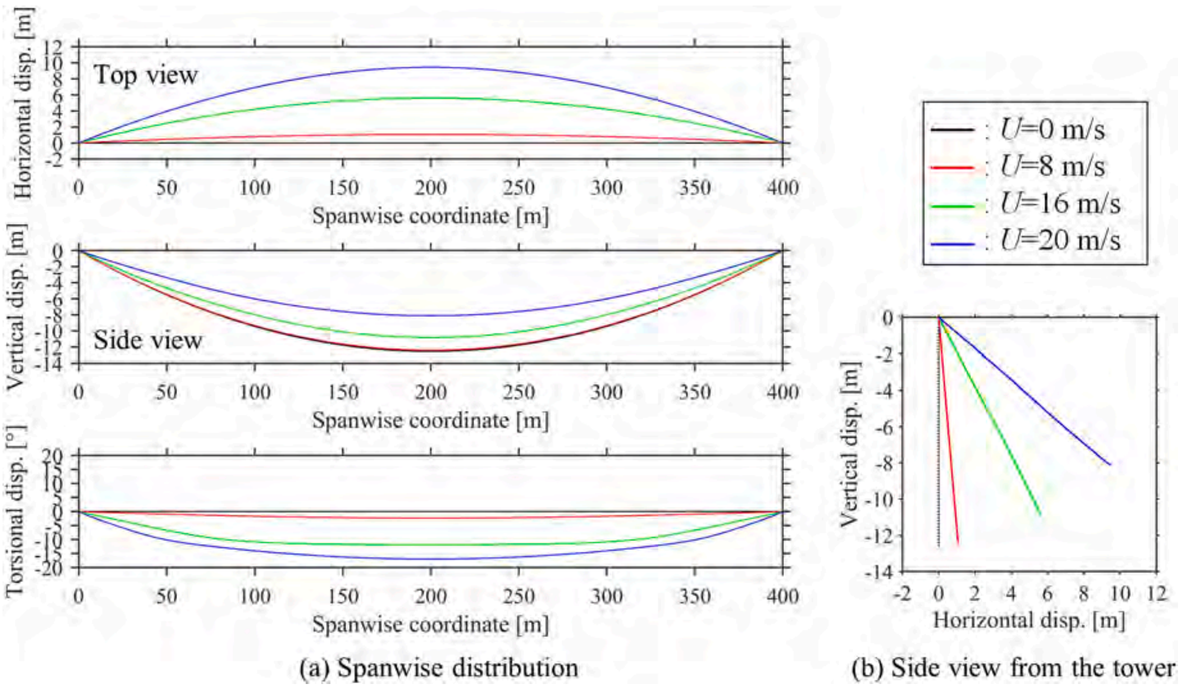

Fig. 15. Bundle static configuration as a function of wind speed (CRIEPI model) for the case of ice shape profile of $+10^{\circ}$.

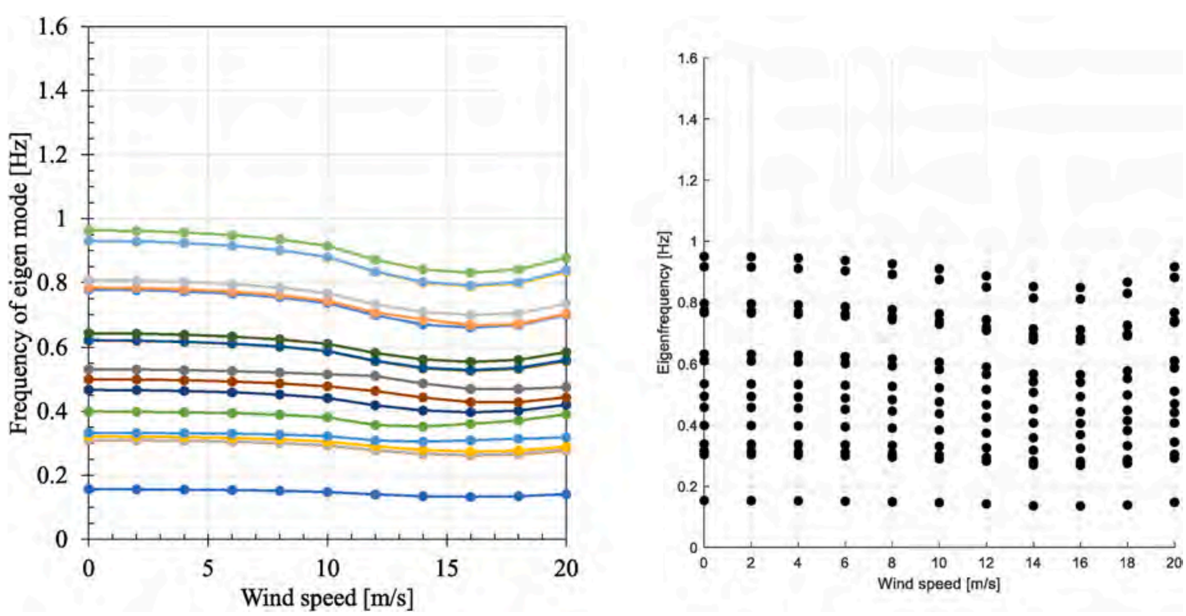

Fig. 16. 10° case, eigenfrequencies VS wind speed: CRIEPI model (left), POLIMI model (right).

couple of unstable modes while CRIEPI model, working in time domain, considers the contribution provided by each mode of vibration. In Table 6, the maximum galloping amplitudes obtained with the two models are reported. The error in the maximum galloping vertical amplitudes, which is the most significant parameter for the design of mitigation devices, is the lowest one. The error in the horizontal amplitude prediction is of the same order of the one obtained for the -10° ice accretion configuration, which demonstrates the robustness and reliability of the two approaches. Lastly, it has to be underlined that the discrepancy found in the torsional amplitude prediction of the $+10^{\circ}$ ice accretion configuration does not influence in a significant way the estimation of the vertical and horizontal components of motion.

5. Conclusions

The paper presented a comparative analysis of the numerical results obtained using two different galloping models. Both the developed models are based on significantly different approaches: the first model relies on a full non-linear FE model running in time domain, while the second computes with a nonlinear FE model only the static equilibrium position as a function of wind speed and the galloping amplitudes are computed with an energy balance method. Both models use the QST to define the motion dependent aerodynamic forces. A 400m single span of four bundled conductor was considered as benchmark case. A triangular ice shape, whose aerodynamic coefficients are known by previous experiments in the wind tunnel, was assumed as ice accretion. Two

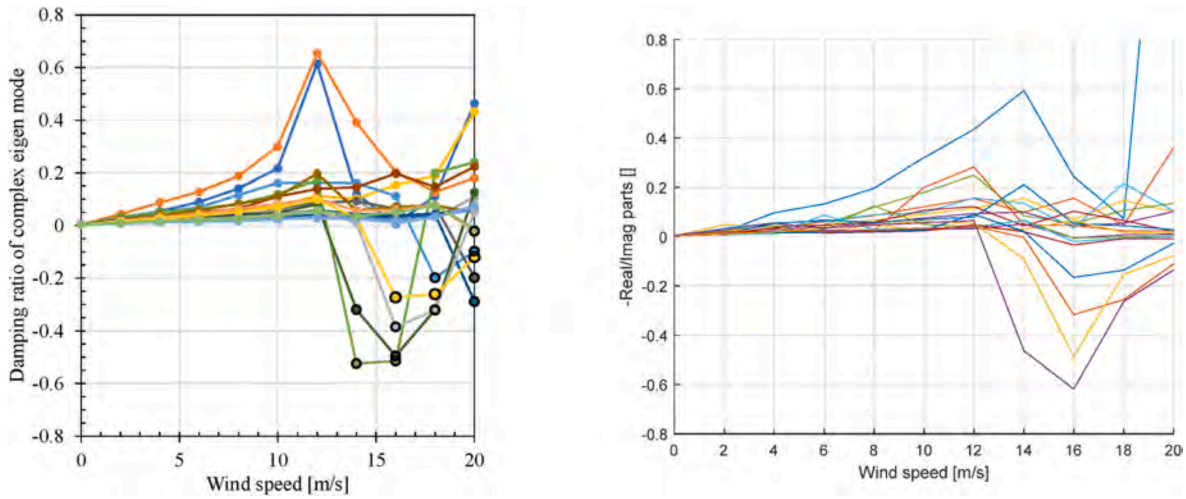

Fig. 17. 10° case, damping ratio VS wind speed: CRIEPI model (left), POLIMI model (right).

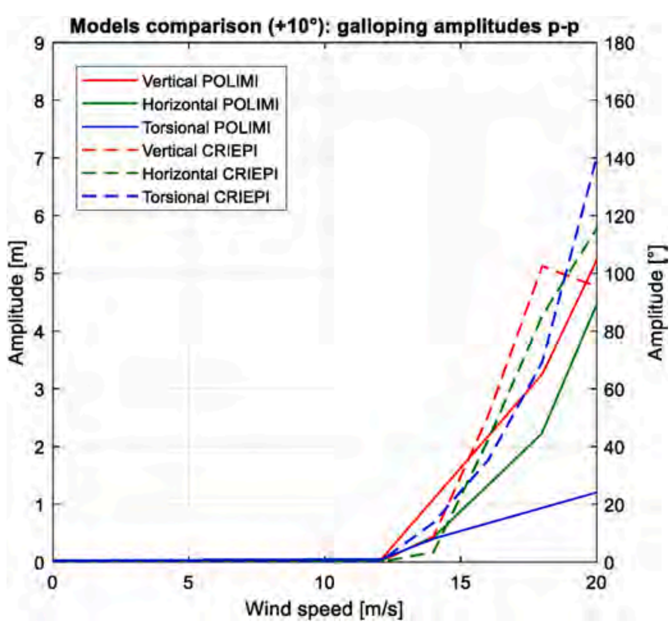

Fig. 18. +10° case, models comparison in terms of galloping amplitudes VS wind speed (continuous lines: POLIMI results; dashed lines: CRIEPI results).

Table 6
Comparison of the galloping amplitudes estimated at 20 m/s by the two models and relative errors.

Ice shape	Model	Vertical [m]	Horizontal [m]	Torsional [°]
+10°	CRIEPI	4.77	5.78	140.37
	Polimi	5.24	4.48	24.19
	Error [%]	−10 %	+22 %	+83 %

configurations of ice accretion were considered in the benchmark: one with an upward tilt of 10° (+10°) from the horizontal direction and another with a downward tilt of 10° (−10°).

Although the two numerical approaches are significantly different, the analyses reported and discussed in the paper show a good agreement in the predicted values of wind speed at which instability occurs and also in the values of maximum galloping amplitudes. In particular, the predicted galloping onset and amplitude trends are very similar for the two models. The error in the maximum galloping amplitude estimation is consistent between the two ice accretion configurations, highlighting the robustness of both approaches to different inputs. In addition, the maximum vertical galloping amplitude is estimated by the two models with a maximum error of 11 %. This result confirms the reliability of the two numerical approaches in providing useful information for the development of mitigation strategies against galloping of conductors in overhead transmission lines.

In conclusion, the results of this benchmark can be taken as a reference for any model that researchers can develop to obtain ice galloping prediction.

CRediT authorship contribution statement

Federico Zanelli: Data curation, Formal analysis, Investigation, Visualization, Writing – original draft, Writing – review & editing. **Giuseppe Bucca:** Data curation, Formal analysis, Investigation, Writing – original draft, Validation. **Stefano Melzi:** Conceptualization, Formal analysis, Investigation, Software, Visualization, Validation. **Sonia Zuin:** Formal analysis, Investigation, Software, Methodology. **Giorgio Diana:** Funding acquisition, Investigation, Methodology, Project administration, Resources, Supervision, Writing – review & editing, Conceptualization. **Saki Taruishi:** Data curation, Formal analysis, Investigation, Software, Visualization, Writing – original draft. **Hisato Matsumiya:** Conceptualization, Funding acquisition, Investigation, Methodology, Project administration, Resources, Supervision, Writing – review & editing.

Declaration of competing interest

The authors declare that they have no known competing financial interests or personal relationships that could have appeared to influence the work reported in this paper.

Data availability

Data will be made available on request.

References

Argentini, T., Rocchi, D., Somaschini, C., Spinelli, U., Zanelli, F., Larsen, A., 2022. Aeroelastic stability of a twin-box deck: comparison of different procedures to assess the effect of geometric details. J. Wind Eng. Ind. Aerod. 220, 104878. https://doi.org/10.1016/j.jweia.2021.104878. October 2021.

Blevins, R.D., Iwan, W.D., 1975. Galloping response of a two-degree-of-freedom system. Am. Soc. Mech. Eng. (75-APMW-9), 1113–1118.

Chabart, O., Lilien, J.L., 1998. Galloping of electrical lines in wind tunnel facilities. J. Wind Eng. Ind. Aerod. 74 (76), 967–976. https://doi.org/10.1016/S0167-6105(98)00088-9.
CIGRE International Council on Large Electrical Systems, 2007. State of the Art of Conductor Galloping. *CIGRE Publication. Technical Brochure no. 322*.
Den Hartog, J.P., 1932. Transmission line vibration due to sleet. Transaction of American Institute of Electrical Engineers 51 (4), 1074–1076.
Diana, G., Resta, F., Zasso, A., Belloli, M., Rocchi, D., 2004. Forced motion and free motion aeroelastic tests on a new concept dynamometric section model of the Messina suspension bridge. J. Wind Eng. Ind. Aerod. 92 (6), 441–462. https://doi.org/10.1016/j.jweia.2004.01.005.
Diana, G., Manenti, A., Melzi, S., 2021. Energy method to compute the maximum amplitudes of oscillation due to galloping of iced bundled conductors. IEEE Trans. Power Deliv. 36 (5), 2804–2813. https://doi.org/10.1109/TPWRD.2020.3027157.
EPRI, P.A., 2009. EPRI: Transmission Line Reference Book: Wind-Induced Conductor Motion, second ed.
Gonzalez-Fernandez, D., Rezgui, D., De Risi, R., Macdonald, J.H.G., Matsumiya, H., Titurus, B., 2025. Identification and analysis of experiment-driven model for galloping in multi-conductor transmission lines. Eng. Struct. 326 (April 2024), 119344. https://doi.org/10.1016/j.engstruct.2024.119344.
Henghold, W.M., Russell, J.J., 1976. Equilibrium and natural frequencies of cable structures. Comput. Struct. 6, 267–271.
Keutgen, R., Lilien, J.L., 2000. Benchmark cases for galloping with results obtained from wind tunnel facilities - validation of a finite element model. IEEE Trans. Power Deliv. 15 (1), 367–374. https://doi.org/10.1109/61.847275.
Liu, X., Min, G., Cai, M., Yan, B., Wu, C., 2021. Two simplified methods for galloping of iced transmission lines. KSCE J. Civ. Eng. 25 (1), 272–290. https://doi.org/10.1007/s12205-020-0693-y.
Lu, J., et al., 2019. Study on wind tunnel test and galloping of iced quad bundle conductor. Cold Reg. Sci. Technol. 160 (November 2018), 273–287. https://doi.org/10.1016/j.coldregions.2018.12.009.
Matsumiya, H., Nishihara, T., Shimizu, M., 2011. Aerodynamic characteristics of ice and snow accreted conductors of overhead transmission lines. In: Proc. 13th Int. Conf. Wind Eng..
Matsumiya, H., Nishihara, T., Yagi, T., 2018. Aerodynamic modeling for large-amplitude galloping of four-bundled conductors. J. Fluid Struct. 82, 559–576. https://doi.org/10.1016/j.jfluidstructs.2018.08.003.
Matsumiya, H., Taruishi, S., Shimizu, M., Sakaguchi, G., Macdonald, J.H.G., 2021. Equivalent static wind loads on snow-accreted overhead wires. Struct. Eng. Int. 32, 78–91. https://doi.org/10.1080/10168664.2021.1967255.
Matsumiya, H., Yukino, T., Shimizu, M., Nishihara, T., 2022a. Field observation of galloping on four-bundled conductors and verification of countermeasure effect of loose spacers. J. Wind Eng. Ind. Aerod. 220 (July 2021), 104859. https://doi.org/10.1016/j.jweia.2021.104859.
Matsumiya, H., Yagi, T., Macdonald, J.H.G., 2022b. Unsteady aerodynamic force modelling for 3-DoF-galloping of four-bundled conductors. J. Fluid Struct. 112, 103581. https://doi.org/10.1016/j.jfluidstructs.2022.103581.
Mou, Z., Yan, B., Lin, X., Huang, G., Lv, X., 2020. Prediction method for galloping features of transmission lines based on FEM and machine learning. Cold Reg. Sci. Technol. 173 (August 2019), 103031. https://doi.org/10.1016/j.coldregions.2020.103031.
Shimizu, M., 2010. "Extensions and applications of an analysis code CAFSS for transmission lines galloping. " CRIEPI Res. Rep. N10027 (in Japanese).
Shimizu, M., Sato, J., 2005. Galloping simulation and observation of a 4-conductor bundle transmission line. In: Proceedings of 4th European-African Conference on Application of Wind Engineering. Prague, Czech Republic.
Shimizu, M., Shugo, M., Sato, J., 1998. "A geometric nonlinear analysis of transmission lines' galloping. J. Struct. Eng. 44a, 951–960 (in Japanese).
Taruishi, S., Matsumiya, H., 2023. Investigation of effect of galloping countermeasures for four-bundled conductors through field observations. Cold Reg. Sci. Technol. 214 (June), 103962. https://doi.org/10.1016/j.coldregions.2023.103962.
Taruishi, S., Matsumiya, H., Matsushima, H., Shimizu, M., 2021. Evaluation of validity of method for making FEM model of a four-bundled conductor by excitation tests and simulations. In: Second International Symposium on Dynamics and Aerodynamics of Cables, pp. 183–190.
The Institute of Electrical Engineers of Japan, 2001. "Analysis techniques for galloping phenomena in overhead transmission lines (in Japanese). Tech. Rep. (844) Power and.
Zanelli, F., Mauri, M., Castelli-Dezza, F., Tarsitano, D., Manenti, A., Diana, G., 2022. Analysis of wind-induced vibrations on HVTL conductors using wireless sensors. Sensors 22 (21), 8165. https://doi.org/10.3390/s22218165.